RSC Advances

PAPER

Cite this: *RSC Adv.*, 2018, **8**, 23323

Novel Eu^{3+}-activated $Ba_2Y_5B_5O_{17}$ red-emitting phosphors for white LEDs: high color purity, high quantum efficiency and excellent thermal stability†

G. Annadurai,[a] Balaji Devakumar,[a] Heng Guo,[ab] R. Vijayakumar,[a] Bin Li,[a] Liangling Sun,[a] Xiaoyong Huang,*[ab] Kai Wang*[b] and Xiao Wei Sun*[b]

Eu^{3+}-activated $Ba_2Y_5B_5O_{17}$ ($Ba_2Y_{5-x}Eu_xB_5O_{17}$; $x = 0.1–1$) red-emitting phosphors were synthesized by the conventional high temperature solid-state reaction method in an air atmosphere. Powder X-ray diffraction (XRD) analysis confirmed the pure phase formation of the as-synthesized phosphors. Morphological studies were performed using field emission-scanning electron microscopy (FE-SEM). The photoluminescence spectra, lifetimes, color coordinates and internal quantum efficiency (IQE) as well as the temperature-dependent emission spectra were investigated systematically. Upon 396 nm excitation, $Ba_2Y_{5-x}Eu_xB_5O_{17}$ showed red emission peaking at 616 nm which was attributed to the $^5D_0 \rightarrow {}^7F_2$ electric dipole transition of Eu^{3+} ions. Meanwhile, the influences of different concentrations of Eu^{3+} ions on the PL intensity were also discussed. The optimum concentration of Eu^{3+} ions in the $Ba_2Y_{5-x}Eu_xB_5O_{17}$ phosphors was found to be $x = 0.8$. The concentration quenching mechanism was attributed to the dipole–dipole interaction and the critical distance (R_c) for energy transfer among Eu^{3+} ions was determined to be 5.64 Å. The asymmetry ratio [($^5D_0 \rightarrow {}^7F_2$)/($^5D_0 \rightarrow {}^7F_1$)] of $Ba_2Y_{4.2}Eu_{0.8}B_5O_{17}$ phosphors was calculated to be 3.82. The fluorescence decay lifetimes were also determined for $Ba_2Y_{5-x}Eu_xB_5O_{17}$ phosphors. In addition, the CIE color coordinates of the $Ba_2Y_{4.2}Eu_{0.8}B_5O_{17}$ phosphors ($x = 0.653$, $y = 0.345$) were found to be very close to the National Television System Committee (NTSC) standard values ($x = 0.670$, $y = 0.330$) of red emission and also showed high color purity (~94.3%). The corresponding internal quantum efficiency of the $Ba_2Y_{4.2}Eu_{0.8}B_5O_{17}$ sample was measured to be 47.2%. Furthermore, the as-synthesized phosphors exhibited good thermal stability with an activation energy of 0.282 eV. The above results revealed that the red emitting $Ba_2Y_{4.2}Eu_{0.8}B_5O_{17}$ phosphors could be potential candidates for application in near-UV excited white light emitting diodes.

Received 10th April 2018
Accepted 23rd May 2018

DOI: 10.1039/c8ra03059f

rsc.li/rsc-advances

1. Introduction

In recent times, scientific research has been focused on new illumination sources to meet the demands of energy conservation and environmental issues.[1] Solid-state lighting (SSL) is a major revolution in the lighting industry.[2] Among SSL, inorganic phosphor-converted white light-emitting diodes (pc-WLEDs) are found to prevail in the lighting market owing to an extensive range of applications in versatile fields, such as flat panel displays, WLEDs, bio-markers, solid state lasers, sensors, and high energy radiation detectors.[3–10] In particular, WLEDs have attracted much attention due to their better performance such as high luminous efficiency, long operational lifetime, high rendering indices, compactness, low-cost, energy saving and environmental protection to surpass traditional incandescent and fluorescent lamps.[11,12]

The most currently used WLEDs are fabricated by the combination of InGaN-based blue LED chips with the yellow emitting $Y_3Al_5O_{12}:Ce^{3+}$ ($YAG:Ce^{3+}$) phosphors.[13] However, there exist some drawbacks in its practical application, such as poor color rendering index ($R_a < 80$), and the high correlated color temperature (CCT ~ 7750 K) owing to the lack of a red spectral component in the visible region.[4,14] In order to obtain high-efficiency WLEDs with appropriate CCT, high CRI and better color stability, alternative method is proposed, which combines the near-ultraviolet (n-UV) LED chips with a mixture of red, green and blue emitting phosphors.[9] There are some commercial $BaMgAl_{10}O_{17}:Eu^{2+}$ (blue), $SrSi_2O_2N_2:Eu^{2+}$ and $Ba_2SiO_4:Eu^{2+}$ (green) phosphors, but a high-efficiency, low-cost red-emitting phosphor is still needed.[2,15,16] The red-emitting phosphors are an essential component for creating high-quality white light.

[a]*Key Lab of Advanced Transducers and Intelligent Control System, Ministry of Education and Shanxi Province, College of Physics and Optoelectronics, Taiyuan University of Technology, Taiyuan 030024, P. R. China. E-mail: huangxy04@126.com*
[b]*Department of Electrical and Electronic Engineering, Southern University of Science and Technology, Shenzhen 518055, P. R. China. E-mail: wangk@sustc.edu.cn; sunxw@sustc.edu.cn*

† Electronic supplementary information (ESI) available. See DOI: 10.1039/c8ra03059f

Currently, the lanthanide-activated sulfide and nitride (*e.g.*, $Y_2O_2S:Eu^{3+}$, $SrGa_2S_4:Eu^{2+}$, $CaS:Eu^{2+}$, $Sr_2Si_5N_8:Eu^{2+}$ and $CaAlSiN_3:Eu^{2+}$) red phosphors are extensively being used for WLEDs.[4,12] However, the commercially available red-emitting sulfide phosphors are chemically unstable with low luminous efficiency. Meanwhile, the nitride based phosphors have critical synthesis conditions, such as high temperature (>1800 °C) and high pressure (0.5 MPa N_2 pressure).[12,13,17,18] The search for non-toxic and highly efficient host materials has attracted researchers. Therefore, it is an urgent task to investigate new red-emitting phosphors for WLEDs with high efficiency, excellent thermal stability and high color purity, which can be excited by n-UV LEDs.

Rare earth ions activated inorganic materials have attractive optical properties because of their distinctive intra-configurational f → f transitions.[9] Among all the rare earth ions, Eu^{3+} ion is the most often used red-emitting activator and exhibits a series of characteristic sharp emissions ascribed to the electronic transitions of $^5D_0 \rightarrow {}^7F_J$ ($J = 0$, 1, 2, 3, and 4).[19–24] Furthermore, the Eu^{3+} ion is expected to be one of the most hopeful species that offers optical devices in the red color region and numerous investigations have been executed in different host materials such as silicates[25] and phosphates[26,27] for the WLEDs application.

As an essential member of the family of luminescent materials, rare earth ions activated borate compounds have been widely investigated, due to their special structure, low sintering temperature, good physical and chemical stability, low cost, excellent optical damage threshold, large band gap, and strong absorption in the n-UV region.[28–30] Recently, blue-emitting $Ba_2Y_5B_5O_{17}:Ce^{3+}$ (ref. 31) and green-emitting $Ba_2Y_5B_5O_{17}:Ce^{3+},Tb^{3+}$ (ref. 32) phosphors have been reported. Zhang *et al.* investigated the $Ce^{3+}/Tb^{3+}/Eu^{3+}$ tri-doped $Ba_2Y_5B_5O_{17}$ multi-color emitting phosphors.[33]

The searching of high-performance red-emitting phosphors for WLEDs, we have systematically investigated in detail luminescence properties of Eu^{3+} activated $Ba_2Y_5B_5O_{17}$ red emitting phosphors. To the best of our knowledge, the elaborated spectroscopic properties of Eu^{3+} singly doped $Ba_2Y_5B_5O_{17}$ and its potential application in WLEDs have not yet been reported. The phosphors showed intense red emission peaking at 616 nm under a 396 nm excitation. The $Ba_2Y_{4.2}Eu_{0.8}B_5O_{17}$ phosphor was found to show the highest emission intensity with internal quantum efficiency (IQE) of 47.2%. Moreover, the $Ba_2Y_{4.2}Eu_{0.8}B_5O_{17}$ phosphor also exhibited good thermal stability and high color purity of red emission. The obtained results suggest that the $Ba_2Y_5B_5O_{17}:Eu^{3+}$ phosphor has potential application for n-UV-pumped WLEDs.

2. Experimental

2.1. Materials and synthesis

Polycrystalline samples of $Ba_2Y_{5-x}Eu_xB_5O_{17}$ ($x = 0$–1.0) phosphors were synthesized using conventional high temperature solid-state reaction method. Stoichiometric amounts of starting materials $BaCO_3$ (Analytical Reagent, A.R.), Y_2O_3 (99.99%), H_3BO_3 (A.R.) and Eu_2O_3 (99.99%) were weighed, and ground using an agate mortar and pestle to form homogeneous mixtures. The obtained mixtures were then transferred into an alumina crucible and pre-heated at 450 °C for 4 h in air. After that, the samples were reground and sintered in air at 1200 °C for 8 h. Finally, the as-prepared samples were gradually cooled down to room temperature in the furnace and were re-ground into homogeneous powder for further measurements.

2.2. Measurements and characterization

The crystalline phase formation of as-synthesized samples were identified by the powder X-ray diffraction (XRD) patterns using Bruker D8 advance powder diffractometer operated at 40 kV and 40 mA with CuKα radiation ($\lambda = 1.5406$ Å). The measurements were carried out in the diffraction angle (2θ) ranging from 10 to 80° with a scanning step of 0.02°. The structural parameters of $Ba_2Y_5B_5O_{17}$ and $Ba_2Y_{4.2}Eu_{0.8}B_5O_{17}$ were refined by the Rietveld refinement method using FullProf_Suite program. The morphology and elemental mapping analyzes of the phosphors were performed using a field-emission scanning electron microscope (FE-SEM; MAIA3 TESCAN). The photoluminescence (PL) and photoluminescence excitation (PLE) spectra as well as the decay curves were recorded using Edinburgh FS5 spectrofluorometer equipped with a 150 W continuous wavelength Xenon lamp and a pulsed Xenon lamp as the excitation source. The IQE of sample was measured by employing a barium sulfate coated integrating sphere attached to the Edinburgh FS5 spectrofluorometer. All the above measurements were carried out at room temperature. Furthermore, the temperature-dependent PL spectra of the phosphors within the temperature range from 303 to 483 K were obtained on the same instrument with a temperature controlling system.

3. Results and discussion

3.1. Phase identification

The XRD patterns of the $Ba_2Y_{5-x}Eu_xB_5O_{17}$ ($x = 0$, 0.1, 0.4, 0.6, 0.8, and 1.0) phosphors are shown in Fig. 1(a). All the observed diffraction peaks of the as-obtained samples were well consistent with the Powder Diffraction File (PDF No. 00-056-0113) for $Ba_2Y_5B_5O_{17}$, and also matched well with the reference data.[33] No other phase or impurity were noticed in the compositions, and the result distinctly suggested that the as-prepared samples were in single phase and Eu^{3+} doping did not significantly influence the crystalline structure of the host due to the similar valence and ionic radius of Eu^{3+} and Y^{3+} [Eu^{3+} ($r = 1.07$ Å), Y^{3+} ($r = 1.02$ Å)].[33] In the meantime, a small shift in the diffraction peaks were observed after increasing Eu^{3+} content, (depicted in Fig. 1(b)) because of the ionic radius between Y^{3+} and Eu^{3+} [Y^{3+} ($r = 1.02$ Å), Eu^{3+} ($r = 1.07$ Å)]. According to previous report, the $Ba_2Y_5B_5O_{17}$ crystallizes as an orthorhombic structure with the space group *Pbcn* (no. 60).[31–33] In order to investigate the crystal structure, the structural parameters of $Ba_2Y_5B_5O_{17}$ and $Ba_2Y_{4.2}Eu_{0.8}B_5O_{17}$ were refined by the Rietveld refinement method using FullProf_Suite program. The observed, calculated and difference of XRD patterns were shown in Fig. 2(a) and (b). The structural parameters are listed in Table 1. All of the observed

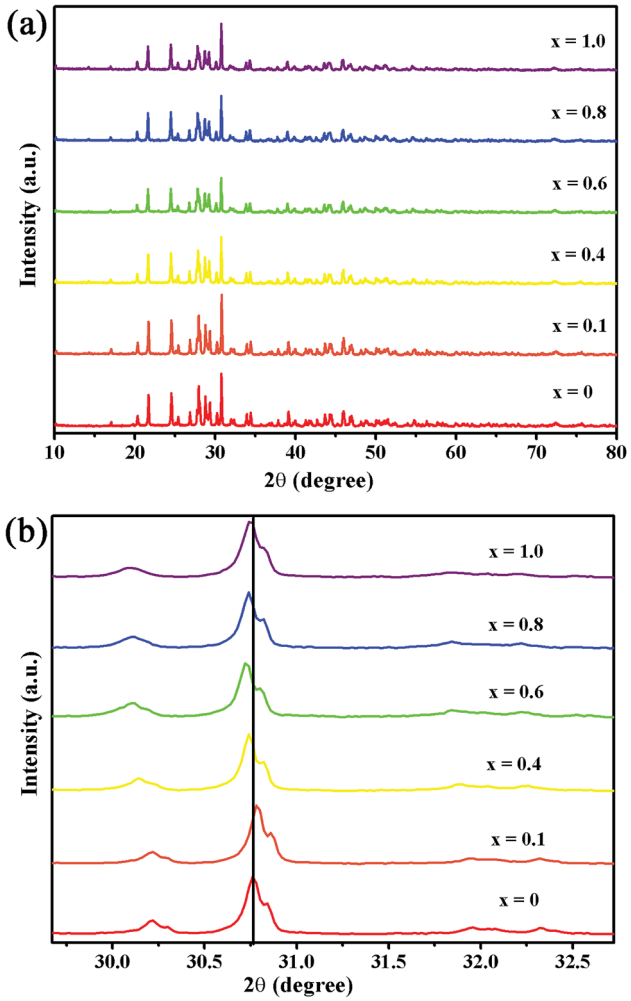

Fig. 1 (a) XRD patterns of as-prepared $Ba_2Y_{5-x}Eu_xB_5O_{17}$ (x = 0, 0.1, 0.4, 0.6, 0.8 and 1.0) phosphors. (b) Magnified XRD patterns for $Ba_2Y_{5-x}Eu_xB_5O_{17}$ (x = 0, 0.1, 0.4, 0.6, 0.8 and 1.0) phosphors.

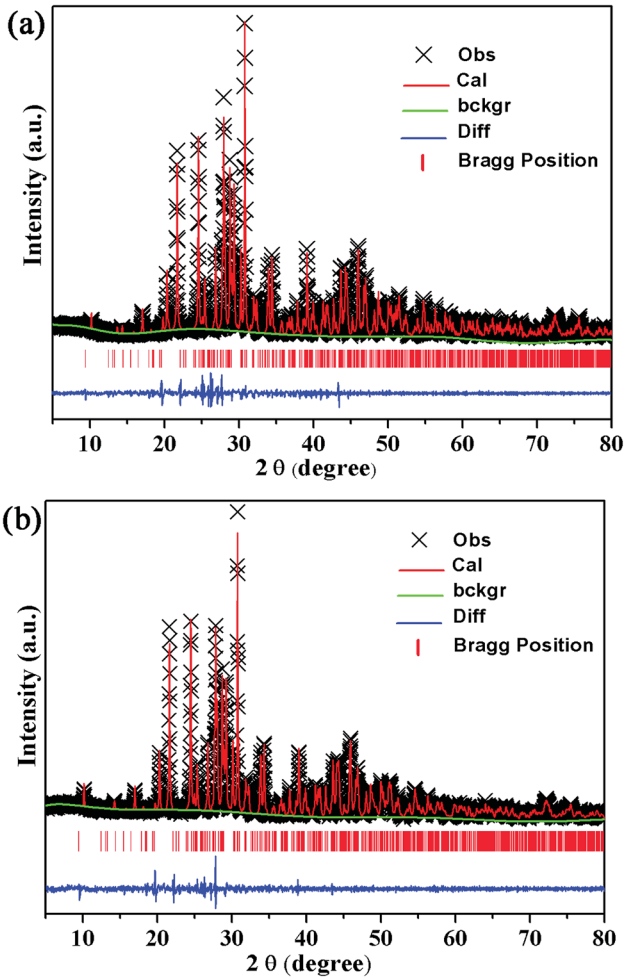

Fig. 2 Rietveld refinement of observed, calculated and difference of the powder XRD patterns of (a) $Ba_2Y_5B_5O_{17}$ and (b) $Ba_2Y_{4.2}Eu_{0.8}B_5O_{17}$.

diffraction peaks showed a good agreement between observed and calculated patterns. The results reveals that $Ba_2Y_5B_5O_{17}$ crystallizes as an orthorhombic structure with space group *Pbcn* (no. 60), and its lattice parameters were determined to be a = 17.4486(8) Å, b = 6.64715(29) Å and c = 13.0128(6) Å and V = 1509.28(19) Å^3. The refinement factors finally converged to R_p = 2.54%, and R_{wp} = 3.67%, which was shown in Table S1 (ESI†). Similarly, the refinement results confirms that the cell parameters of $Ba_2Y_{4.2}Eu_{0.8}B_5O_{17}$, a = 17.45484(18) Å, b = 6.66655(9) Å, c = 13.06090(18) Å and V = 1519.813(34) Å^3, the refinement factors finally converged to R_p = 1.99%, and R_{wp} = 2.70%. The atomic coordinates were provided in the Table 2. Furthermore, the unit cell structure of $Ba_2Y_5B_5O_{17}$ is depicted in Fig. 3.

As reported previously, the $Ba_2Y_5B_5O_{17}$ host lattice contains two crystallographically independent, fully occupied Y^{3+} sites. Specifically, a distorted octahedron and a distorted capped trigonal prism around Y_3 and Y_4 site. The two Y^{3+} sites are shared with Ba^{2+}, namely, Ba_1/Y_1 with a majority Ba (CN = 10) and Y_2/Ba_2 with a majority Y (CN = 7), respectively. All of the boron atoms are three-coordinated by oxygen, making slightly distorted trigonal planar units.[31–33]

3.2. Morphology analysis

Fig. 4(a) and (b) depicts the FE-SEM micrographs of the $Ba_2Y_{4.2}Eu_{0.8}B_5O_{17}$ phosphors. The as-obtained micrographs exposed that the particles were agglomerated with irregular morphology. The estimated size of the particles could be in micrometer range which is suitable practical application for WLEDs.[34] Meanwhile, the elemental mapping results also suggested that the Eu were evenly distributed throughout the entire particles, as indicated in Fig. 4(c). The remaining mapping images of Ba, Y, B, and O was provided in Fig. S1 (ESI†).

3.3. Photoluminescence properties

Fig. 5 shows the PLE and PL spectra of the $Ba_2Y_{4.2}Eu_{0.8}B_5O_{17}$ phosphors. The excitation spectrum was monitored at 616 nm corresponding to $^5D_0 \rightarrow {}^7F_2$ transition of Eu^{3+}. The PLE spectrum consisted of two parts namely a broad excitation band in the wavelength range from 230 to 310 nm, and a series of sharp PLE peaks located between 315 to 550 nm. It can be clearly noted that the broad band centered at 277 nm was assigned to the $O^{2-} \rightarrow Eu^{3+}$ charge transfer band (CTB), corresponding to the electron transfer from the completely filled 2p orbital of O^{2-}

Table 1 Crystal structure data of $Ba_2Y_5B_5O_{17}$ and $Ba_2Y_{4.2}Eu_{0.8}B_5O_{17}$ from the Rietveld refinement

Compound	$Ba_2Y_5B_5O_{17}$	$Ba_2Y_{4.2}Eu_{0.8}B_5O_{17}$
Crystal system	Orthorhombic	Orthorhombic
Space group	*Pbcn* (no. 60)	*Pbcn* (no. 60)
a (Å)	17.4486 (8)	17.45484 (18)
b (Å)	6.64715 (29)	6.66655 (9)
c (Å)	13.0128 (6)	13.06090 (18)
$\alpha = \beta = \gamma$ (°)	90	90
V (Å^3)	1509.28 (19)	1519.813 (34)
Z	4	4
R_p (%)	2.54	1.99
R_{wp} (%)	3.67	2.70

ions to the empty states of 4f orbital of Eu^{3+} ions. In addition, the several sharp excitation peaks, associated with the typical intra-configurational 4f–4f forbidden transitions of Eu^{3+} ions were found with peaks positioned at 321 nm ($^7F_0 \rightarrow {}^5H_6$), 364 nm ($^7F_0 \rightarrow {}^5D_4$), 383 nm ($^7F_0 \rightarrow {}^5L_7$), 396 nm ($^7F_0 \rightarrow {}^5L_6$), 418 nm ($^7F_0 \rightarrow {}^5D_3$), 466 nm ($^7F_0 \rightarrow {}^5D_2$) and 537 nm ($^7F_0 \rightarrow {}^5D_1$).[9,30,35] Among all the sharp PLE peaks, the strongest excitation peak located at 396 nm matches well with the n-UV LED chip for WLEDs applications. The PL spectrum of $Ba_2Y_{4.2}Eu_{0.8}B_5O_{17}$ phosphor ($\lambda_{ex} = 396$ nm) exhibited the well-known emission characteristics of Eu^{3+} in the spectral region from 500 nm to 750 nm. The sharp emission peaks at 580, 592, 616, 650 and 705 nm can be assigned to the transitions from the excited state $^5D_0$ to ground state ^7F_J ($J = 0, 1, 2, 3$ and 4) levels of Eu^{3+} ions.[30,36] From this spectrum, it can be ascertained that the intensity of electric dipole (ED) $^5D_0 \rightarrow {}^7F_2$ transition at around 616 nm was much higher than that of the magnetic dipole (MD) $^5D_0 \rightarrow {}^7F_1$ transition at around 592 nm. When the Eu^{3+} ion is situated at the crystallographic site with inversion symmetry, the $^5D_0 \rightarrow {}^7F_1$ (MD) transition is dominant while in a site without inversion symmetry, the $^5D_0 \rightarrow {}^7F_2$ (ED) transition will be dominant.[37,38] The above result suggested that the local symmetry of Eu^{3+} sites belong to the non-centrosymmetric in $Ba_2Y_5B_5O_{17}$ host lattice.

Table 2 The atomic coordinations, occupancies and isotropic displacement parameters as determined by Rietveld refinement for $Ba_2Y_{4.2}Eu_{0.8}B_5O_{17}$

Atom	x	y	z	Occ.	U_{iso} (Å^2)	Wyck.
Ba_1	0.33581	0.02396	0.18393	0.90943	−0.00532	8d
Y_1	0.33581	0.02396	0.18393	0.90943	−0.00532	8d
Ba_2	0.5	0.41124	0.75	0.2	0.01275	4c
Eu	0.5	0.41124	0.75	0.8	0.01275	4c
Y_3	0.18165	0.04629	0.41451	1	−0.02461	8d
Y_4	0.01607	0.76051	0.47887	1	0.0088	8d
B_1	0.15138	0.52964	0.40624	1	−0.09	8d
O_1	0.19532	0.38553	0.41003	1	−0.072	8d
O_2	0.14487	0.7102	0.40012	1	0.01301	8d
O_3	0.08387	0.45757	0.49893	1	0.0003	8d
B_2	0.69329	0.58445	0.77545	1	−0.06048	8d
O_4	0.67945	0.4438	0.75562	1	0.0293	8d
O_5	0.61289	0.3519	0.8842	1	−0.00301	8d
O_6	0.69615	0.58683	0.91213	1	−0.03713	8d
O_7	0.94229	0.89496	0.5666	1	−0.0122	8d
O_8	0.0274	0.26356	0.67037	1	−0.055	8d
O_9	0.5	0.94764	0.25	1	−0.04744	4c
B_3	0.0	0.63778	0.25	1	−0.09	4c

3.4. Concentration quenching and energy transfer of $Ba_2Y_{5-x}Eu_xB_5O_{17}$ phosphors

The PL spectra of $Ba_2Y_{5-x}Eu_xB_5O_{17}$ ($0.1 \leq x \leq 1.0$) phosphors with different Eu^{3+} concentrations under 396 nm excitation were shown in Fig. 6(a). The shapes and peak positions of the PL spectra remained unchanged with different concentration of Eu^{3+} ions, except for the PL intensity (see Fig. 6(b)). The inset of Fig. 6(a) illustrates the dependence of PL intensity of various Eu^{3+} concentrations under $\lambda_{ex} = 396$ nm. It can be seen that the PL intensity enhanced with the amount of Eu^{3+} until it reached a maximum intensity at $x = 0.8$, followed by a gradual decrease with a further increase in Eu^{3+} ion content owing to the concentration quenching effect.[13] In general, the concentration quenching phenomenon commonly takes place as a consequence of exchange interaction, radiation re-absorption or multipole–multipole interaction. In addition, the non-radiative energy transfer mechanism among Eu^{3+} ions is strongly dependent on the critical transfer distance (R_c), which was calculated by using the concentration quenching method. The R_c can be calculated according to the equation proposed by Blasse:[39]

$$R_c \approx 2\left(\frac{3V}{4\pi x_c N}\right)^{1/3} \quad (1)$$

where V represents the volume of the unit cell, x_c is the critical concentration of Eu^{3+} ions, and N is the number of host cations in the unit cell. In the case of $Ba_2Y_{5-x}Eu_xB_5O_{17}$ phosphors, the values of V, x_c and N were 1509.28 Å^3, 0.8 and 20, respectively,[32,33] and thus the R_c was determined to be 5.64 Å. The short-distance exchange interaction becomes ineffective when the critical distance is larger than 5 Å. The radiation re-absorption is unlikely to take place as there is no overlap between PL and PLE spectra in the present case. Therefore, the concentration quenching mechanism of Eu^{3+} ions in $Ba_2Y_5B_5O_{17}$ system was dominated by the multipole–multipole interaction. There are three types of electric multipole interactions, including dipole–dipole (d–d), dipole–quadrupole (d–q)

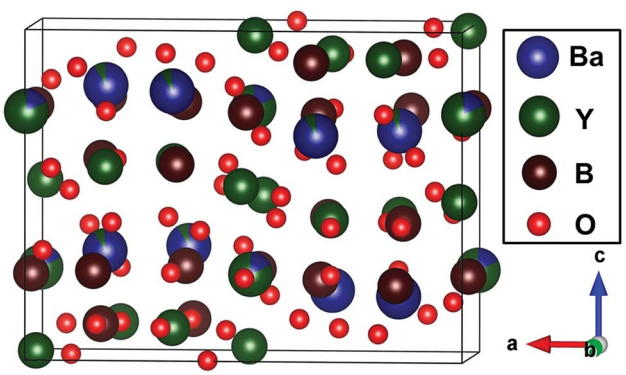

Fig. 3 Crystal structure of $Ba_2Y_5B_5O_{17}$.

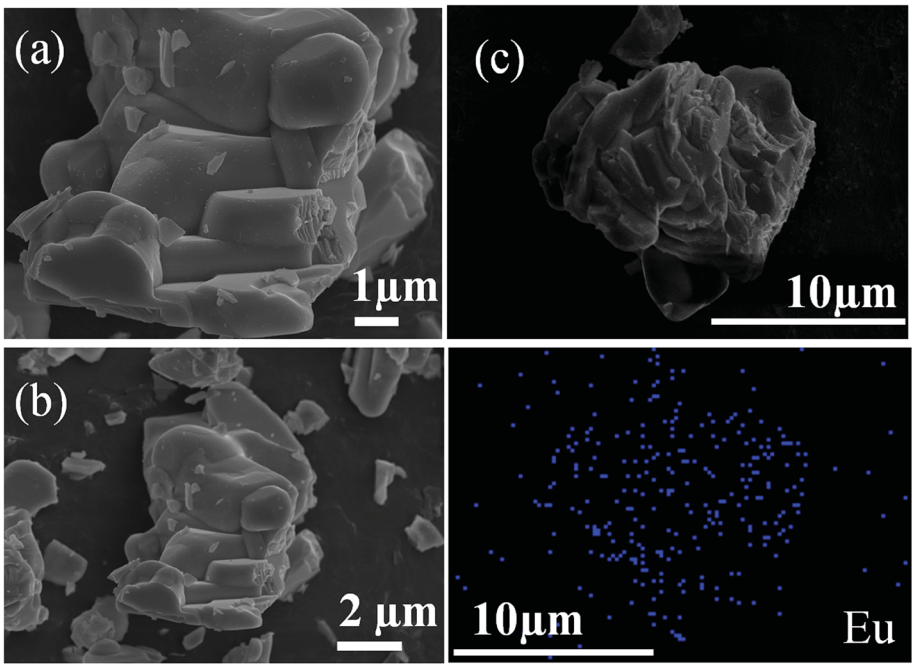

Fig. 4 FE-SEM micrographs (a) and (b). The elemental mapping (c) of europium for the $Ba_2Y_{4.2}Eu_{0.8}B_5O_{17}$ phosphors.

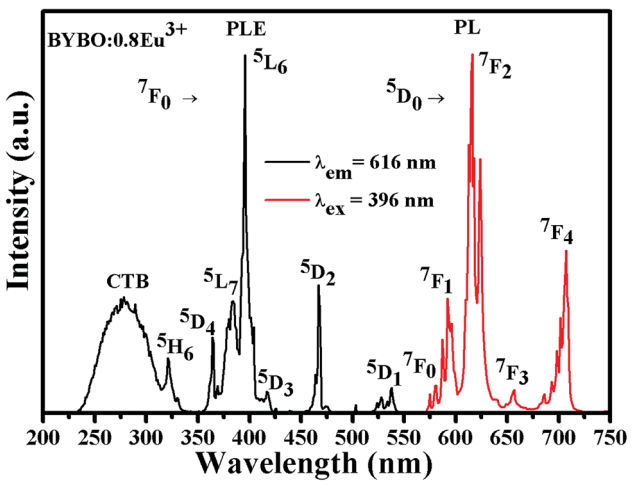

Fig. 5 The PLE (λ_{em} = 616 nm) and PL (λ_{ex} = 396 nm) spectra of $Ba_2Y_{4.2}Eu_{0.8}B_5O_{17}$ phosphors.

or quadrupole–quadrupole (q–q). Based on Dexter's theory,[40] the emission intensity (I) per activator ion can be determined by the following equation:

$$\frac{I}{x} = k\left[1 + \beta(x)^{\theta/3}\right]^{-1} \quad (2)$$

where I/x represents the emission intensity per activator concentration, x stands for the Eu^{3+} ions concentration; k and β are constants for the given host under the same excitation conditions; θ is a function of multipolar interaction, and $\theta = 6$, 8 and 10 corresponds to d–d, d–q or q–q interactions, respectively.[41] The above mentioned equation can be rearranged further by assuming $\beta(x) \gg 1$:[42]

$$\log\left(\frac{I}{x}\right) = K' - \frac{\theta}{3}\log(x) \quad (3)$$

where $K' = \log k - \log \beta$. The dependence of $\log(I/x)$ on $\log(x)$, as shown in Fig. 7, which was found to be linear and the slope was determined to be −1.91369. Therefore, the value of θ can be calculated as ~5.74, which approximately equals to 6, indicating that the non-radiative energy transfer mechanism among the Eu^{3+} ions can be ascribed to d–d interaction in $Ba_2Y_{5-x}Eu_xB_5O_{17}$ phosphors.

Generally, the ED transition $^5D_0 \rightarrow {}^7F_2$ is a hypersensitive transition as this type of transition is very sensitive to the local environment, while the MD transition $^5D_0 \rightarrow {}^7F_1$ is insensitive to the local environment at Eu^{3+} site.[38,43] Meanwhile, the ratio of integrated emission intensity (asymmetry ratio (R)) of ED ($^5D_0 \rightarrow {}^7F_2$) to MD ($^5D_0 \rightarrow {}^7F_1$) transitions can be used to evaluate the site symmetry around the Eu^{3+} ions. In general, the high value of $R > 1$ indicates that the local symmetry around Eu^{3+} ion is non-centrosymmetric.[44] Fig. 8 shows the plot of integrated emission intensity [($^5D_0 \rightarrow {}^7F_2$)/($^5D_0 \rightarrow {}^7F_1$)] ratio values on different Eu^{3+} concentrations. The R values decreased with increasing Eu^{3+} ion concentration. The calculated R values were found to be 4.36, 4.16, 4.02, 3.95, 3.89, 3.83, 3.80, 3.82, 3.80 and 3.83 for different concentration of ($0.1 \le x \le 1.0$) Eu^{3+} activated phosphors, indicating that Eu^{3+} occupied the distorted cation sites with non-centrosymmetric.[44] Particularly, the calculated R value (3.82) of $Ba_2Y_{4.2}Eu_{0.8}B_5O_{17}$ phosphors was found to be practically better than several previous Eu^{3+}-doped red phosphors, as shown in Table 3. The lack of an inversion center the Eu^{3+} ion is favorable in achieving a bright red phosphor with high color purity.[36]

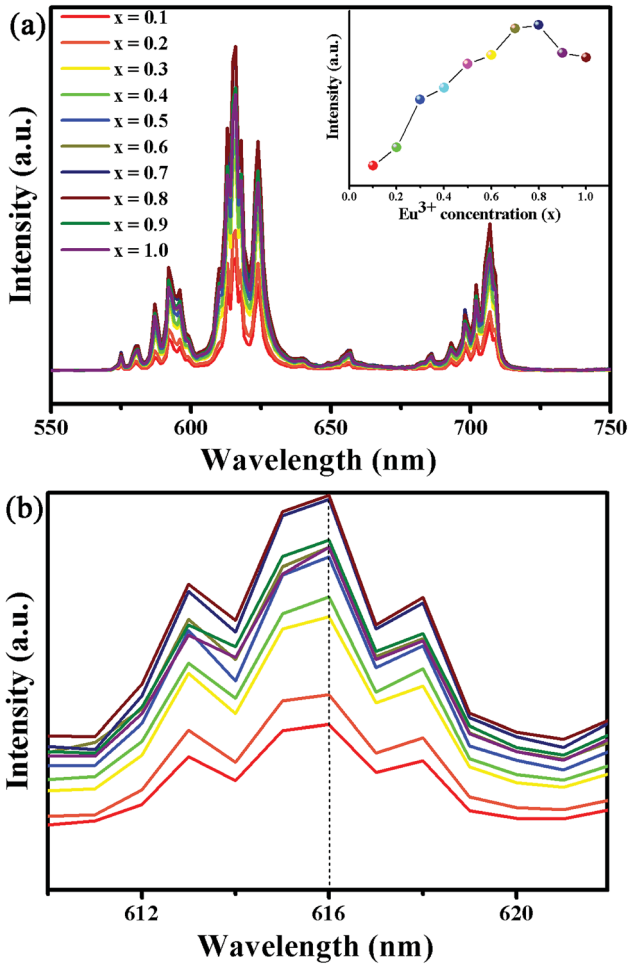

Fig. 6 (a) The PL spectra of $Ba_2Y_{5-x}Eu_xB_5O_{17}$ ($0.1 \leq x \leq 1.0$) phosphors under 396 nm excitation. The inset shows the corresponding PL intensity as a function of Eu^{3+} concentrations (x). (b) The magnified PL spectra for $Ba_2Y_{5-x}Eu_xB_5O_{17}$ ($0.1 \leq x \leq 1.0$) phosphors.

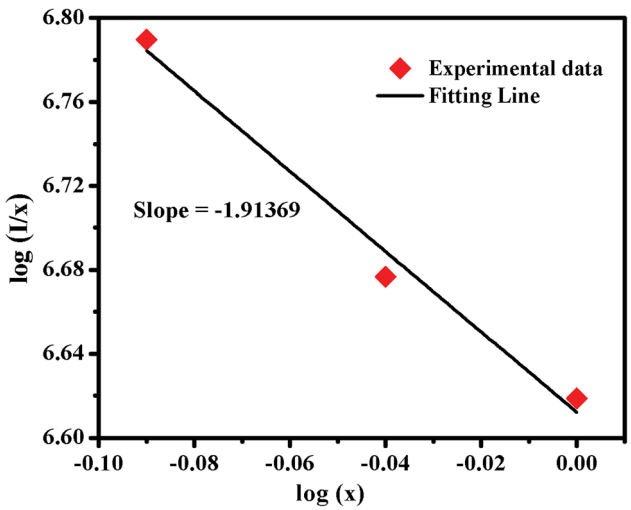

Fig. 7 Dependence of $\log(I/x)$ on $\log(x)$ for $Ba_2Y_{5-x}Eu_xB_5O_{17}$ phosphors ($\lambda_{ex} = 396$ nm).

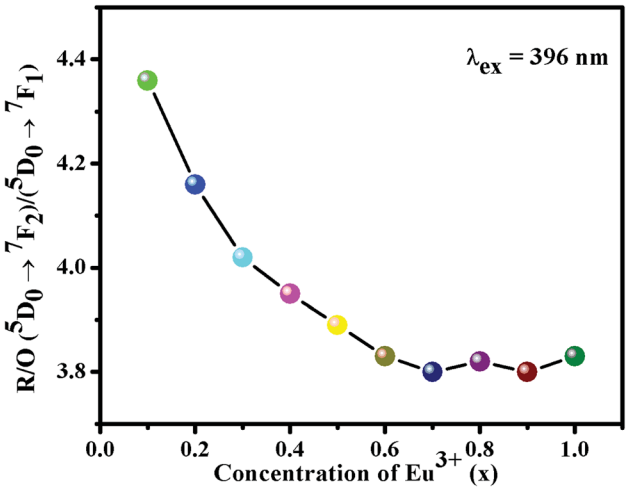

Fig. 8 The asymmetry ratio (R) values with various concentrations of Eu^{3+} in $Ba_2Y_{5-x}Eu_xB_5O_{17}$ ($0.1 \leq x \leq 1.0$) phosphors.

3.5. PL decay curves of $Ba_2Y_{5-x}Eu_xB_5O_{17}$ phosphors

Fig. 9 illustrates the room-temperature PL decay curves of $Ba_2Y_{5-x}Eu_xB_5O_{17}$ phosphors with different Eu^{3+} concentrations ($0.1 \leq x \leq 1.0$) under excitation at 396 nm and monitored at 616 nm. All the decay curves can be fitted well based on a first-order exponential decay function as given by the following equation:

$$I(t) = I_0 + A\exp(-t/\tau) \quad (4)$$

where $I(t)$ and I_0 are the luminescence intensities at time t and $t = 0$, respectively; A is a constant, and τ represents the characteristic decay lifetime for the exponential component.[9,13] According to eqn (4), the calculated lifetime values of the $^5D_0$ emitting level of Eu^{3+} ions in $Ba_2Y_{5-x}Eu_xB_5O_{17}$ ($0.1 \leq x \leq 1.0$) phosphors were 1.347, 1.365, 1.388, 1.426, 1.461, 1.484, 1.519, 1.546, 1.580 and 1.593 ms, respectively. Obviously, the PL lifetime values slightly increased with increasing various Eu^{3+} concentrations, which can be attributed to energy migration between Eu^{3+} ions.[13,45–47]

3.6. The CIE chromaticity coordinates of $Ba_2Y_{4.2}Eu_{0.8}B_5O_{17}$

Fig. 10 presents the CIE chromaticity diagram of $Ba_2Y_{4.2}Eu_{0.8}B_5O_{17}$ phosphors under excitation at 396 nm. According to the PL spectrum, the CIE coordinates were calculated as (0.653, 0.345), which was much closer to the NTSC standard red light (0.670, 0.330) than that of the commercial red-emitting phosphor of $Y_2O_2S:Eu^{3+}$ (0.637, 0.327) and better than other Eu^{3+} activated phosphors $Na_3Sc_2(PO_4)_3:0.35Eu^{3+}$ (0.642, 0.353) $Ca_{0.9}Eu_{0.1}TiO_3$ (0.630, 0.370) $CaLa_{0.65}Eu_{0.35}B_7O_{13}$ (0.611, 0.388).[9,48,49] Furthermore, to better understand the red emission of the Eu^{3+}-activated $Ba_2Y_{4.2}Eu_{0.8}B_5O_{17}$ phosphors, the color purity was calculated according to the following expression:[9,50]

$$\text{Color purity} = \frac{\sqrt{(x-x_i)^2+(y-y_i)^2}}{\sqrt{(x_d-x_i)^2+(y_d-y_i)^2}} \times 100\% \quad (5)$$

where (x, y), (x_i, y_i) and (x_d, y_d) refers the color coordinates of emission light, the equal energy point and color coordinates of

Table 3 Asymmetry ratio (R) of ($^5D_0 \rightarrow {}^7F_2/{}^5D_0 \rightarrow {}^7F_1$) transitions of Eu^{3+} activated different red phosphors

Red phosphors	Asymmetry ratio (R) ($^5D_0 \rightarrow {}^7F_2/{}^5D_0 \rightarrow {}^7F_1$)	Ref.
$Ba_2Y_{4.2}Eu_{0.8}B_5O_{17}$	3.82	This work
$NaSrB_5O_9$:7%Eu^{3+}	2.73	5
$Ba_2CaZn_2Si_6O_{17}$:0.9Eu^{3+}	2.36	6
$Li_6Y(BO_3)_3$:0.5%Eu^{3+}	1.71	7
$BaTa_2O_6$:30%Eu^{3+}	1.40	8
$Na_3Sc_2(PO_4)_3$:0.35Eu^{3+}	1.37	9

the dominant wavelength points, respectively. In the present work, ($x = 0.653$, $y = 0.345$), ($x_i = 0.310$, $y_i = 0.316$,) and ($x_d = 0.675$, $y_d = 0.324$). According to eqn (5), the color purity of $Ba_2Y_{4.2}Eu_{0.8}B_5O_{17}$ red phosphors was determined to be around

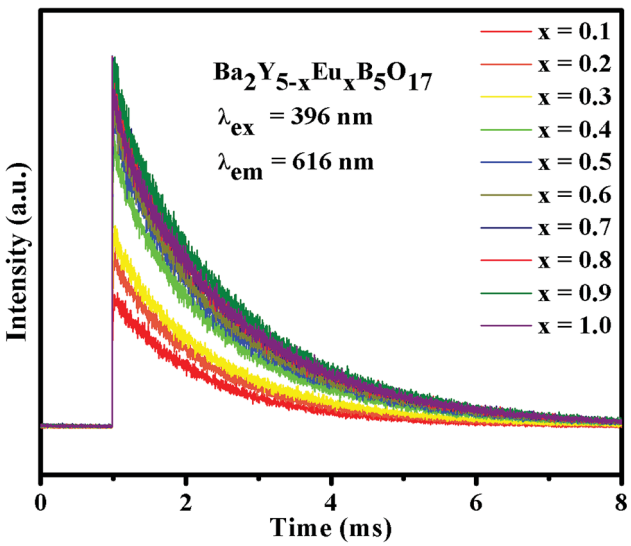

Fig. 9 PL decay curves of $Ba_2Y_{5-x}Eu_xB_5O_{17}$ ($0.1 \leq x \leq 1.0$) phosphors excited at 396 nm and monitored at 616 nm.

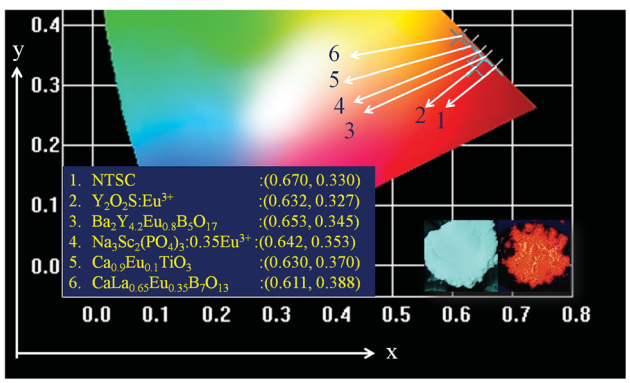

Fig. 10 CIE color coordinates of the NTSC, commercial $Y_2O_2S:Eu^{3+}$, $Ba_2Y_{4.2}Eu_{0.8}B_5O_{17}$, $Na_3Sc_2(PO_4)_3$:0.35Eu^{3+}, $Ca_{0.9}Eu_{0.1}TiO_3$ and $CaLa_{0.65}Eu_{0.35}B_7O_{13}$ red phosphors. The inset shows the digital photographs of $Ba_2Y_{4.2}Eu_{0.8}B_5O_{17}$ phosphors at daylight (left) and under the 365 nm UV lamp (right).

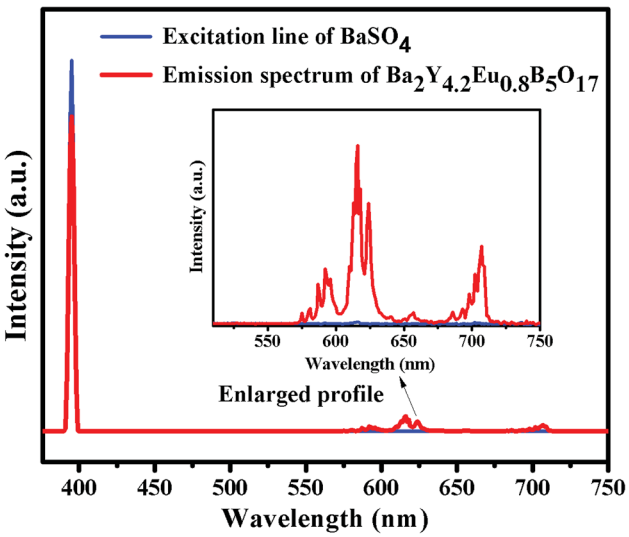

Fig. 11 Excitation line of $BaSO_4$ and emission spectrum of the $Ba_2Y_{4.2}Eu_{0.8}B_5O_{17}$ phosphors recorded by a spectrofluorometer equipped with an integrating sphere. The inset shows the magnified emission spectrum in the wavelength range 500–750 nm.

94.3%. We can find that the $Ba_2Y_{4.2}Eu_{0.8}B_5O_{17}$ phosphor showed strong red emission intensity with good CIE chromaticity coordinates and eminent color purity. In addition, the IQE is an essential parameter for practical application. The IQE of the optimized phosphor was measured using an integrating sphere. The IQE value can be calculated according to the equation:[51,52]

$$\eta_{QE} = \frac{\int L_S}{\int E_R - \int E_S} \quad (6)$$

where L_S is the luminescence emission spectrum of the sample, E_S is the spectrum of the light used for exciting the sample, and E_R is the spectrum of the excitation light without the sample in the sphere, respectively (see Fig. 11). Under the excitation of 396 nm, the IQE of $Ba_2Y_{4.2}Eu_{0.8}B_5O_{17}$ red-emitting phosphor was determined to be 47.2%, which was higher than the commercial $Y_2O_2S:Eu^{3+}$ phosphors (IQE: 35%).[4,9] These results suggest that the $Ba_2Y_{5-x}Eu_xB_5O_{17}$ phosphor could be a promising red phosphor for n-UV-based WLEDs.

3.7. Thermal stability of the Eu^{3+}-activated $Ba_2Y_{4.2}Eu_{0.8}B_5O_{17}$ phosphors

The thermal stability of phosphor is one of the essential parameter to find potential application in the high-power WLEDs.[13] Fig. 12(a) shows the PL spectra of $Ba_2Y_{4.2}Eu_{0.8}B_5O_{17}$ phosphors recorded at various temperatures ranging from 303–483 K under excitation at 396 nm. The spectra clearly indicated that the PL intensity decreased with increasing temperature owing to thermal quenching effect. Generally, the PL intensity of phosphors at 423 K with respect to that at room temperature (303 K) is utilized to assess the thermal stability.[9] It is evident that the PL intensity decreased to 68.7% at 423 K in comparison with that of its initial PL intensity at room temperature (303 K), as shown in Fig. 12(b). To better understand the temperature

effect on the PL intensity of the phosphors, the activation energy was calculated according to the Arrhenius equation, which can be illustrated below:[9]

$$I(T) = \frac{I_0}{1 + c\exp\left(-\frac{\Delta E_a}{kT}\right)} \quad (7)$$

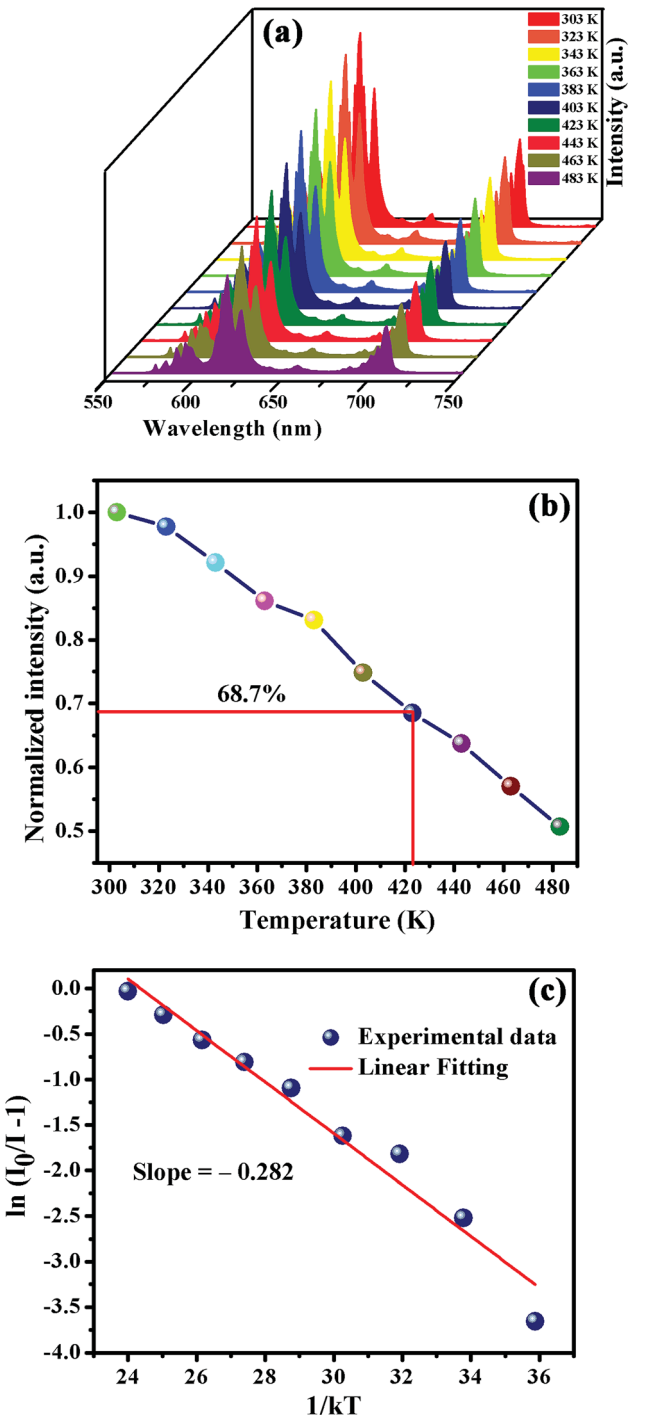

Fig. 12 (a) Temperature dependent PL spectra of $Ba_2Y_{4.2}Eu_{0.8}B_5O_{17}$ phosphor (λ_{ex} = 396 nm). (b) Normalized PL intensity of $Ba_2Y_{4.2}Eu_{0.8}B_5O_{17}$ phosphors as a function of different temperatures. (c) The relationship of $\ln(I_0/I - 1)$ *versus* $1/kT$ of the $Ba_2Y_{4.2}Eu_{0.8}B_5O_{17}$ phosphors.

where I_0 and $I(T)$ stands for the initial PL intensity and the PL intensity at different given temperature T, ΔE_a represents the activation energy for thermal quenching, c is a constant for the host, and k is the Boltzmann constant (8.629×10^{-5} eV K^{-1}). The value of ΔE_a can be estimated through the eqn (8) which is modified by the eqn (7) as follows:[53]

$$\ln\left[\left(\frac{I_0}{I}\right) - 1\right] = -\frac{\Delta E_a}{kT} + \ln c \quad (8)$$

The plot of $\ln[(I_0/I) - 1]$ *versus* $1/kT$ yielded a straight line, as illustrated in Fig. 12(c). The slope of the fitting line is around −0.282 and thus the activation energy ΔE_a was determined to be 0.282 eV for $Ba_2Y_{4.2}Eu_{0.8}B_5O_{17}$ phosphors, which was higher than the other Eu^{3+} activated $Na_3Sc_2(PO_4)_3$, $Ca_3La(GaO)_3(BO_3)_4$ and $BaZrGe_3O_9:Eu^{3+}$ red phosphors (ΔE_a: 0.23,0.25 and 0.175 eV).[9,37,54] This high activation energy suggested that the obtained phosphors have good thermal stability and thus they are suitable for applying in WLEDs.

4. Conclusion

In summary, Eu^{3+}-activated $Ba_2Y_{5-x}Eu_xB_5O_{17}$ ($0.1 \leq x \leq 1.0$) red emitting phosphors have been synthesized by a high-temperature solid-state reaction. Under excitation at 396 nm, the $Ba_2Y_{5-x}Eu_xB_5O_{17}$ phosphors exhibited intense red emission at 616 nm due to the electric dipole transition $^5D_0 \rightarrow {}^7F_2$ of Eu^{3+}. The optimum concentration of Eu^{3+} in the $Ba_2Y_{5-x}Eu_xB_5O_{17}$ phosphor was determined to be $x = 0.8$. The corresponding concentration quenching mechanism was evidenced to be d–d interaction. Meanwhile, the $Ba_2Y_{4.2}Eu_{0.8}B_5O_{17}$ red phosphor also exhibited impressive thermal stability, which showed about 68.7% at 423 K of its initial emission intensity at room temperature 303 K. As a result, the optimal $Ba_2Y_{4.2}Eu_{0.8}B_5O_{17}$ phosphor presented significant red emission intensity, excellent color purity with color coordinates (0.653, 0.345) and the IQE of 47.2%. These results imply that the $Ba_2Y_{4.2}Eu_{0.8}B_5O_{17}$ phosphors can serve as potential red emitting phosphors for n-UV pumped WLEDs.

Conflicts of interest

There are no conflicts to declare.

Acknowledgements

This work was supported by the National Natural Science Foundation of China (No. 51502190, 61674074, 51402148 and 61405089), National Key Research and Development Program of China administrated by the Ministry of Science and Technology of China (No. 2016YFB0401702), Shenzhen Peacock Team Project (No. KQTD2016030111203005), Shenzhen Innovation Project (No. JCYJ20160301113356947, JCYJ20160301113537474, JCYJ20150630145302223), Distinguished Young Scholar of Natural Science Foundation of Guangdong (No. 2017B030306010), Foshan Innovation Project (No. 2014IT100072), the start-up fund from Southern University of

Science and Technology, and the Open Fund of the State Key Laboratory of Luminescent Materials and Devices (South China University of Technology, No. 2017-skllmd-01).

References

1 X. Wang, Z. Zhao, Q. Wu, Y. Li and Y. Wang, *Inorg. Chem.*, 2016, **55**, 11072–11077.
2 M. Janulevicius, P. Marmokas, M. Misevicius, J. Grigorjevaite, L. Mikoliunaite, S. Sakirzanovas and A. Katelnikovas, *Sci. Rep.*, 2016, **6**, 26098.
3 Z. Xia, C. Ma, M. S. Molokeev, Q. Liu, K. Rickert and K. R. Poeppelmeier, *J. Am. Chem. Soc.*, 2015, **137**, 12494–12497.
4 X. Huang, S. Wang, B. Li, Q. Sun and H. Guo, *Opt. Lett.*, 2018, **43**, 1307–1310.
5 G. Dillip, K. Mallikarjuna, S. Dhoble and B. D. P. Raju, *J. Phys. Chem. Solids*, 2014, **75**, 8–14.
6 G. Annadurai and S. M. M. Kennedy, *J. Lumin.*, 2016, **169**, 690–694.
7 M. M. Yawalkar, G. Zade, K. Dabre and S. Dhoble, *Luminescence*, 2016, **31**, 1037–1042.
8 M. İlhan, M. K. Ekmekçi, A. Mergen and C. Yaman, *J. Fluoresc.*, 2016, **26**, 1671–1678.
9 H. Guo, X. Huang and Y. Zeng, *J. Alloys Compd.*, 2018, **741**, 300–306.
10 X. Huang, B. Li and H. Guo, *J. Alloys Compd.*, 2017, **695**, 2773–2780.
11 X. Zhang, Y. Fu, Z. Zhao, J. Yang, N. Li and M. Zhang, *J. Lumin.*, 2018, **194**, 311–315.
12 H. Zhu, M. Fang, Z. Huang, K. Chen, X. Min, Y. Mao and M. Wang, *J. Lumin.*, 2016, **172**, 180–184.
13 Y. Zhang, W. Gong and G. Ning, *New J. Chem.*, 2016, **40**, 10136–10143.
14 Q. Liu, Z. Zheng, X. Zhang and Z. Bai, *J. Alloys Compd.*, 2015, **628**, 298–302.
15 V. Bachmann, C. Ronda, O. Oeckler, W. Schnick and A. Meijerink, *Chem. Mater.*, 2008, **21**, 316–325.
16 M. A. Lim, J. K. Park, C. H. Kim, H. D. Park and M. W. Han, *J. Mater. Sci. Lett.*, 2003, **22**, 1351–1353.
17 S. Zhang, Y. Hu, L. Chen, X. Wang, G. Ju and Y. Fan, *J. Mater. Res.*, 2013, **28**, 3130–3136.
18 S. Kasturi and V. Sivakumar, *Mater. Chem. Front.*, 2017, **1**, 550–561.
19 Y. Zhang, X. Li, K. Li, H. Lian, M. Shang and J. Lin, *ACS Appl. Mater. Interfaces*, 2015, **7**, 2715–2725.
20 A. Kruopyte, R. Giraitis, R. Juskenas, D. Enseling, T. Jüstel and A. Katelnikovas, *J. Lumin.*, 2017, **192**, 520–526.
21 X. Huang, *Nat. Photonics*, 2014, **8**, 748.
22 P. Du, X. Huang and J. S. Yu, *Chem. Eng. J.*, 2018, **337**, 91–100.
23 H. Deng, Z. Gao, N. Xue, J. H. Jeong and R. Yu, *J. Lumin.*, 2017, **192**, 684–689.
24 Z. Gao, N. Xue, J. H. Jeong and R. Yu, *Mater. Res. Bull.*, 2017, **95**, 497–502.
25 Y. Zhang, J. Xu, Q. Cui and B. Yang, *Sci. Rep.*, 2017, **7**, 42464.
26 D. V. Deyneko, V. A. Morozov, J. Hadermann, A. E. Savon, D. A. Spassky, S. Y. Stefanovich, A. A. Belik and B. I. Lazoryak, *J. Alloys Compd.*, 2015, **647**, 965–972.
27 R. Cao, T. Fu, Y. Cao, H. Ao, S. Guo and G. Zheng, *Mater. Lett.*, 2015, **155**, 68–70.
28 W. Xiao, X. Zhang, Z. Hao, G.-H. Pan, Y. Luo, L. Zhang and J. Zhang, *Inorg. Chem.*, 2015, **54**, 3189–3195.
29 P. Chen, F. Mo, A. Guan, R. Wang, G. Wang, S. Xia and L. Zhou, *Appl. Radiat. Isot.*, 2016, **108**, 148–153.
30 R. Guo, S. Tang, B. Cheng and D. Tan, *J. Lumin.*, 2013, **138**, 170–173.
31 M. Hermus, P.-C. Phan and J. Brgoch, *Chem. Mater.*, 2016, **28**, 1121–1127.
32 Y. Xiao, Z. Hao, L. Zhang, W. Xiao, D. Wu, X. Zhang, G.-H. Pan, Y. Luo and J. Zhang, *Inorg. Chem.*, 2017, **56**, 4538–4544.
33 X. Zhang, J. Zhang and Y. Chen, *Dyes Pigm.*, 2018, **149**, 696–706.
34 B. Han, J. Zhang, Z. Wang, Y. Liu and H. Shi, *J. Lumin.*, 2014, **149**, 150–154.
35 H.-Y. Chen, H.-L. Lai, R.-Y. Yang and S.-J. Chang, *J. Mater. Sci.: Mater. Electron.*, 2016, **27**, 2963–2967.
36 W. Dai, M. Zhou, Z. Xian and L. Zeng, *RSC Adv.*, 2014, **4**, 25470–25478.
37 Q. Zhang, X. Wang, X. Ding and Y. Wang, *Inorg. Chem.*, 2017, **56**, 6990–6998.
38 X. Huang, B. Li, H. Guo and D. Chen, *Dyes Pigm.*, 2017, **143**, 86–94.
39 G. Blasse, *J. Solid State Chem.*, 1986, **62**, 207–211.
40 D. L. Dexter, *J. Chem. Phys.*, 1953, **21**, 836–850.
41 L. Van Uitert, *J. Electrochem. Soc.*, 1967, **114**, 1048–1053.
42 D. Dexter and J. H. Schulman, *J. Chem. Phys.*, 1954, **22**, 1063–1070.
43 P. Du and J. S. Yu, *Dyes Pigm.*, 2017, **147**, 16–23.
44 T. L. Francis, P. P. Rao, M. Thomas, S. Mahesh and V. Reshmi, *J. Mater. Sci.: Mater. Electron.*, 2014, **25**, 2387–2393.
45 A. Fu, A. Guan, F. Gao, X. Zhang, L. Zhou, Y. Meng and H. Pan, *Opt. Laser Technol.*, 2017, **96**, 43–49.
46 J. Grigorjevaite and A. Katelnikovas, *ACS Appl. Mater. Interfaces*, 2016, **8**, 31772–31782.
47 L. Mengting and J. Baoxiang, *J. Rare Earths*, 2015, **33**, 231–238.
48 D. K. Singh and J. Manam, *J. Mater. Sci.: Mater. Electron.*, 2016, **27**, 10371–10381.
49 F. Xiong, J. Luo, H. Lin, X. Meng, Y. Wang, H. Shen and W. Zhu, *Optik*, 2018, **156**, 31–38.
50 P. Du, Y. Guo, S. H. Lee and J. S. Yu, *RSC Adv.*, 2017, **7**, 3170–3178.
51 J. Zhong, D. Chen, Y. Zhou, Z. Wan, M. Ding, W. Bai and Z. Ji, *Dalton Trans.*, 2016, **45**, 4762–4770.
52 T. Wei, Q. Ren, X. Wu, X. Shi, B. Wang and Z. Huo, *Opt. Laser Technol.*, 2016, **85**, 7–13.
53 X. Huang, B. Li and H. Guo, *Ceram. Int.*, 2017, **43**, 10566–10571.
54 J. Liang, P. Du, H. Guo, L. Sun, B. Li and X. Huang, *Dyes Pigm.*, 2018, **157**, 40–46.